applied sciences

MDPI

Article

New Sensor Based on Magnetic Fields for Monitoring the Concentration of Organic Fertilisers in Fertigation Systems

Daniel A. Basterrechea [1], Lorena Parra [1,2], Marta Botella-Campos [1], Jaime Lloret [1,*] and Pedro V. Mauri [2]

[1] Instituto de Investigación para la Gestión Integrada de zonas Costeras, Universitat Politècnica de València, Grao de Gandía, 46730 Valencia, Spain; dabasche@epsg.upv.es (D.A.B.); loparbo@doctor.upv.es (L.P.); marbocam@teleco.upv.es (M.B.-C.)

[2] Instituto Madrileño de Investigación y Desarrollo Rural, Agrario y Alimentario, Finca El Encin, Autovía del Noreste A-2, Km. 38.200, Alcalá de Henares, 28805 Madrid, Spain; pedro.mauri@madrid.org

* Correspondence: jlloret@dcom.upv.es

Received: 11 September 2020; Accepted: 13 October 2020; Published: 16 October 2020

Abstract: In this paper, we test three prototypes with different characteristics for controlling the quantity of organic fertiliser in the agricultural irrigation system. We use 0.4 mm of copper diameter, distributing in different layers, maintaining the relation of 40 spires for powered coil and 80 for the induced coil. Moreover, we develop sensors with 8, 4, and 2 layers of copper. The coils are powered by a sine wave of 3.3 V peak to peak, and the other part is induced. To verify the functioning of this sensor, we perform several simulations with COMSOL Multiphysics to verify the magnetic field created around the powered coil, as well as the electric field, followed by a series of tests, using six samples between the 0 g/L and 20 g/L of organic fertiliser, and measure their conductivity. First, we find the working frequency doing a sweep for each prototype and four configurations. In this case, for all samples, making a sweep between 10 kHz and 300 kHz. We obtained that in prototype 1 (P1) (coil with 8 layers) the working frequency is around 100 kHz, in P2 (coil with 4 layers) around 110 kHz, and for P3 (coil with 2 layers) around 140 kHz. Then, we calibrate the prototypes measuring the six samples at four different configurations for each sensor to evaluate the possible variances. Likewise, the measures were taken in triplicate to reduce the possible errors. The obtained results show that the maximum difference of induced voltage between the lowest and the highest concentration is for the P2/configuration 4 with 1.84 V. Likewise, we have obtained an optimum correlation of 0.997. Then, we use the other three samples to verify the optimum functioning of the obtained calibrates. Moreover, the *ANOVA simple* procedure is applied to the data of all prototypes, in the working frequency of each configuration, to verify the significant difference between the values. The obtained results indicate that there is a significate difference between the average of concentration (g/L) and the induced voltage, and another with a level of 5% of significance Finally, we compare all of the tested prototypes and configurations, and have determined that prototype three with configuration 1 is the best device to be used as a fertiliser sensor in water.

Keywords: inductive coils; precision agriculture; organic fertiliser; inductive sensors; agricultural monitoring; irrigation control

1. Introduction

The world population is growing very fast. The number of people will continue to rise, growing at an average of 1.1% a year up to 2030. Agriculture is becoming very important to supply the

required food necessities, according to the Food and Agriculture Organization (FAO) between 1900 and 2000 year, in a report about the evolution of food, agriculture, and other reliable crop production [1]. According to agricultural indexes, agriculture showed some stability between 1960 and 1980. Nonetheless, after 1980, the values decreased very fast. Thus, agriculture production is not able to sustain the requirements of world food demand, which is becoming a huge problem nowadays.

Agriculture depends entirely on soil for obtaining the highest quality and quantity of food. Soil is a big ecosystem formed by a high amount of microorganisms, such as bacteria and fungi, which takes part in 90% of the decomposition of organic material (OM) [2]. Moreover, soil has different kinds of minerals and nutrients. The three main nutrients are nitrogen (N), phosphorus (P), and potassium (K). Furthermore, other important nutrients are calcium, magnesium, and sulphur. Additionally, plants need small quantities of other elements, known as trace elements [3]. Among all these minerals, one of the most important is nitrogen. Nitrogen interacts with carbon (C) in C/N relation, which is necessary to fix the nitrogen, and to obtain good crop production [4].

In this context, to increase production, farmers are using fertilisers. These compounds are necessary to provide the required nutrients to the soil so that the plants can have all the nutrients they need. This increment in nutrients causes higher production, increasing the harvest [5]. Fertilisers can be divided into three different classes: (i) simple or multi nutrient fertilisers, depending on if they are composed of one or more nutrients; (ii) organic or inorganic; and (iii) fast or low release. Generally, the use of multi nutrient fertilisers is recommended more. Otherwise, the increase of a single nutrient ends up creating new limiting nutrients. Moreover, the use of organic fertilizer (OF) can carry disadvantages if it is not appropriately controlled. The soil must contain oxygen for the correct function of the bacteria. The decrease in oxygen levels is nearly related to the increase of OM [6]. Furthermore, when OF is misused, the runoff occurs, and the OM contaminates the water bodies, such as rivers, lakes, or aquifers [7].

One of the best forms to control the necessities of the crops is the monitoring of irrigation water quality [8]. The monitoring of water has decisive importance because it could incorporate nutrients or compounds into the land. In the case of fertigation systems, irrigation systems, which include fertiliser, the most relevant parameters to control the fertiliser quantity, are the conductivity, turbidity, and, in some cases, the pH. The fertilisers have a percentage of minerals that increase the conductivity of the water. In addition, the OFs have a dark colour and, in solution with water, provokes an increment of the turbidity. Finally, some fertilisers could cause pH variations in the irrigation water. The standard form to monitor the water quality is the extraction of an irrigation water sample, and measuring in the laboratory. The use of a conductivity meter in agriculture is another method for controlling the quality of water. Nevertheless, this type of analyses is not useful since it is not possible to measure the water in situ and obtain continuous measurements. Moreover, this type of methodology has a high economic cost because it is needed for a person to take measures, specialised equipment, and reagents.

Nowadays, the use of sensors for monitoring agriculture parameters is increasing. In this context, different works are being developed. The application of a Wireless Sensor Network (WSN) for monitoring the irrigation for crops is one of the examples of the use of a sensors network in agriculture [9]. The use of technology for monitoring agricultural parameters is known as Precision Agriculture (PA). PA combines the WSN, information systems, enhanced machinery, and informed management to optimise production, by accounting for variability and uncertainties within the agricultural system. This strategy is applied to several agroecosystems [10].

One way to control the amount of fertilisers is by monitoring the soil parameters using different kinds of devices. Venkatesh K.P. Rao [11] developed a grid of micro-mechanical (MEMS) sensors based in a gas detector, which will be able to detect the ammonia presented in fertilisers. The gathered data are provided using the deflection and voltage output from the piezoelectric layer. This is useful for informing the farmers about soil conditions in real-time. Another type of monitoring system is presented by Yuhei Hirono et al. [12]. The system that they present is based on the

monitoring and modelling of nitrogen leaching caused by over-fertilisation. They use a Hydrus- One dimensional (1D) simulation model to obtain data for optimal fertiliser management practices.

Moreover, the application of smart fertilisers is another alternative to control or reduce the amount of nutrient in agricultural soil. Feng et al. [13] proposed a controlled-slow release fertiliser. This "smart" fertiliser is based on polymer brushes of poly (*N*,*N*-dimethyl aminoethyl methacrylate). Boli et al. [14] proposed a similar solution based on slow-release fertilisers. They studied a fertilised with natural attapulgite, clay, ethyl cellulose, film, and sodium carboxymethyl cellulose/hydroxyethyl cellulose hydrogel formulation. Claudine F. Souza et al. [15] developed fertilisers based on biodegradable substances to obtain more sustainable crops. The created fertiliser is composed of biodegradable polymers that release water and nutrients gradually to the environment, without leaving residue.

The improvement of fertigation techniques is crucial in order to have proper management of fertilisers in agricultural lands. In this context, Sharma M.O et al. [16] described a Global System for Mobile Communications (GSM)-based irrigation system with control of soil moisture and water level. They propose the monitoring and control of water and fertiliser with a liquid level detector and different control schemes and monitoring methods. Their system was implemented using the micro-controller 89S52 and Programmable Integrated Circuited (PIC) 18F4550. Finally, Data, Zhang P. et al. [17] proposed a system based on the Internet of Things and other technologies for real-time monitoring. This system will able to predict and forecast the water requirement of crops in the different growth periods and make the decision concerning automatic irrigation and fertilisation. The decision-making is possible by using a model based in Big Data. When selecting a sensor to be part of a WSN for monitoring the presence of OFs in the fertigation systems, it is recommended to use physical devices that do not need maintenance. Chemical sensors—such as the ones used for monitoring the pH—are not the best options to be applied in the field, since they need periodic maintenance to replace some membranes and electrodes or clean the device. Therefore, a turbidity sensor, which is composed of optical devices, is one of the alternatives [18]. The last alternative is the salinity sensor, which could detect changes in the conductivity of the water due to the presence of fertiliser [19]. Regarding conductivity sensors, there are two types of sensors: ones composed of electrodes and ones composed of inductive coils. The latter are preferred due to the absence of electrodes and the possibility of isolating the sensor. The capability of inductive coils for detection of inorganic fertiliser is already demonstrated. These sensors are sensitive to the changes in conductivity, which make them ideal to detect or control fertilisers or other compounds that are conductive [20]. In the same context, a low-cost sensor array based on planar electromagnetic sensors to determine the contamination level of two common fertiliser components—nitrate and sulphate in water sources—is developed [21]. Thus, although no specific physical systems for monitoring OF is found, the use of electromagnetic sensors, such as inductive coils, have been demonstrated for monitoring other compounds in water.

In this paper, the design, calibration, and verification of an inductive sensor to control the quantity of organic fertiliser in water, are presented. The sensors we included in this study are based on prototypes previously developed to detect inorganic fertiliser. In this context, the sensors are going to be applied to measure OF [20], which has a different characteristic than inorganic fertiliser. Moreover, we are going to test a new procedure to power the prototypes, considering the polarity of the generated magnetic field. The proposed sensors are based on two copper coils attached to the same structure. The prototypes used are those that have the best configuration based on previous studies [20]. Our hypothesis is that the induced magnetic field is sensible to the changes of OF concentration. To test our hypothesis, we use nine samples distributed in the range between 0 g/L and 20 g/L. The first step before testing the sensors in the laboratory is to perform several simulations using COMSOL Multiphysics [22] for all three prototypes and different mediums: air, pure water, seawater, and three OF samples. To find the Working Frequency (WF) of the prototypes in the four different configurations, we follow the procedure indicated in [19]. We use six samples to find the WF and

calibrate the prototypes, and another three to verify them. Finally, we perform an ANOVA procedure to verify if the found differences are statistically significant or not, and verify our hypothesis.

The rest of the paper is structured as follows. In Section 2, the state of art (method) and the background are described. Then, the material used in the experiment and the selected methodology to perform the simulations and the tests are detailed in Section 3. Following, Section 4 presents the obtained results of the different prototypes. Finally, the conclusion and future work are outlined in Section 5.

2. State-of-the-Art (Method)

The application of the sensors network to monitor agricultural parameters is a practice that is spreading very fast. In this section, the different related works are going to be exposed. First, the use of electromagnetic sensors for environmental monitoring and the fundamentals of these sensors are detailed. Finally, we will explain the advantages of our experiment compared to others.

2.1. The Use of Electromagnetic Sensors for Environment Monitoring

2.1.1. Background

The first clue of the use of an inductive sensor was the patent of the apparatus for a micro-inductive investigation of earth formations with improved electroquasistic shielding in 1988. This patent was classified as "G01V3/28", electric or magnetic prospecting or detecting, measuring magnetic field characteristics of the earth, e.g., declination, deviation, specially adapted for well-logging, operating with magnetic or electric fields, produced or modified either by the surrounding earth formation or by the detecting device using induction coils [23]. Following, a study using inductive sensors was performed in 1989, with an experiment concerning a non-contacting electrical conductivity sensor for remote, hostile environments. In this study, Kleinberg, R. L. et al. calculated the signal level of the sensor when near the homogenous formation. Equation (1) represented the signal level for the inductive sensor proposed in [24].

$$V_L = 2\pi w^2 \mu^2 I n_I n_r \sigma G \quad (1)$$

Where w is the frequency, μ is the magnetic permeability of the medium, I is the current through the transmitter, n_t and n_r are the number of turns of the transmitter and the receiver coils, respectively, σ is the conductivity of the formation, and G is a geometrical factor and depends on the coil dimensions and the distance to the formation. In our case, the formation is the medium in which the coils are suspended, water with fertiliser, and its μ and σ will change as the concentration of fertiliser increases, due to the increase of positive and negative charges of molecules of the fertiliser. The study performed in [25] characterised the circular inductive coils, and studied the effects of signal noise, temperature, and pressure on the device. Finally, they concluded that these sensors are accurate and optimum for conductivity monitoring in hostile environments.

On the other hand, the prototypes proposed in this paper are composed of sensors that use the phenomenon of mutual inductance. This principle states that, when in a situation where there is a powered coil (PC), powered with an electric current (EC), a magnetic field will appear. This magnetic field depends on several parameters, such as the number of spires (N) of the coil, the diameter of the wire (ØW), the diameter of the powered coil (ØPC), and the used signal to power the coil (including the voltage and the frequency). According to Ampère's Law, the magnetic flux density (B) of a solenoid depends on the permeability of the core (μ_0), the number of spires (N), and the intensity of the current (I), as shows Equation (1). Nonetheless, Equation (2) is for an infinite solenoid in free space. In our case, the solenoid is introduced in the water, which has its relative permeability (μ_r). Therefore, the length of the solenoid (l) should be included, as shown in Equation (3). We expect an increase in the permeability of the water when OF is added. Since the permeability of a medium is a measure of its resistance to the creation of a magnetic field, if permeability increases, the magnetic field will increase. Moreover, the increase of the magnetic field, which is maximum in the centre of the solenoid where the

ferromagnetic core is generally placed, will have an effect on the electrical conductivity of the medium and increase the flow of electrons. In our device, the magnetic field will be higher in the centre of the powered solenoid and the core will be water with different amounts of fertiliser.

$$B = \mu_0 NI \tag{2}$$

$$B = \mu_0 \mu_r NI/l \tag{3}$$

If there is another coil in the proximity of the PC, the aforementioned magnetic field will cause that coil to be induced. This phenomenon is known as mutual inductance. The lines from the magnetic field of the PC will go through the induced coil (IC), thus creating a magnetic flux. The theoretical description of the mutual inductance can be seen in [26]. If the medium in which the magnetic flux goes through is modified, for example, changing the amount of OF diluted in water, the output voltage should change. The mutual inductance, M, of two solenoids, can be described by Equation (4). Where L1 and L2 are the inductances of each coil, and k is the coupling coefficient. L1 and L2 depend on the core ($\mu_0\mu_r$), the amount of turns N, the cross-sectional area A in m^2, and the length of the solenoid l, as shown in Equation (5). Therefore, the mutual inductance depends on the medium of the core. In our case, the water. When the permeability of the water changes, the coupling effect k changes. The value of k is maximum (1) when the coils are perfectly coupled and minimum (0) when there is no inductive coupling. When k is 1, it means that 100% of the lines of flux of PC cuts all the turns of the IC, it is assumed high permeability of the water and coils with perfect geometry. In our experiments, the characteristics of the core (permeability) are one of the studied factors. Moreover, the testing of different prototypes is aimed to evaluate the effect of different geometries. The position of coils is a fixed factor. However, the distance between the PC and IC and the total length of both coils changes from one prototype to another.

$$M = k\sqrt{L1\ L2} \tag{4}$$

$$L1 = \frac{\mu_0\ \mu_r\ N\ A}{l} \tag{5}$$

According to the experiments performed in previous works [26], the induced voltage will depend on the characteristics of the coil, such as N, ØW, and the diameter of the induced coil (ØIC). Moreover, the induced voltage, also known as the Vout, depends on the B and μ_r. Generally, this principle is used with coils that have a ferromagnetic core, and is the principle of the power transformers.

The magnetic flux density is determined by the Biot–Savart law presented in Equation (6) and depends on the permeability μ, a time varying current denoted by $i(t)$, the distance to the source R, and the unit vector $\vec{R}$ [27].

$$d\vec{B} = \frac{\mu}{4\pi}\frac{i(t)\,\overrightarrow{dl} \times \vec{R}}{R^3} \tag{6}$$

Furthermore, it is possible to obtain the induced electric field using Faraday's law, represented by Equation (7). Faraday's law states that a time varying magnetic flux, $d\Phi$ induces an electric field around a closed path. Taking into account Stokes's theorem, the induced electric field can be written in terms of the number of turns, N, in a non-varying surface, dS [28].

$$\oint_C \vec{E} \cdot d\vec{l} = \frac{-d}{dt}\int_S \vec{B} \cdot dS \tag{7}$$

$$\oint_C \vec{E} \cdot d\vec{l} = -N\ \frac{-d\Phi}{dt} \tag{8}$$

In Figure 1, we show a summary of the considered variables in our experiments. According to the polarisation of the PC and its relative position to the IC, when the generated magnetic field increases, the Vout can increase or decrease. In our experiments, we maintain the same polarisation in each coil. Furthermore, to limit the number of variables in our tests, the input signal (the signal to

power the PC) will have two fixed parameters, intensity and voltage; and one variable parameter (frequency). This is done based on the results of [26] when the authors showed that each combination of coils has different peak frequencies.

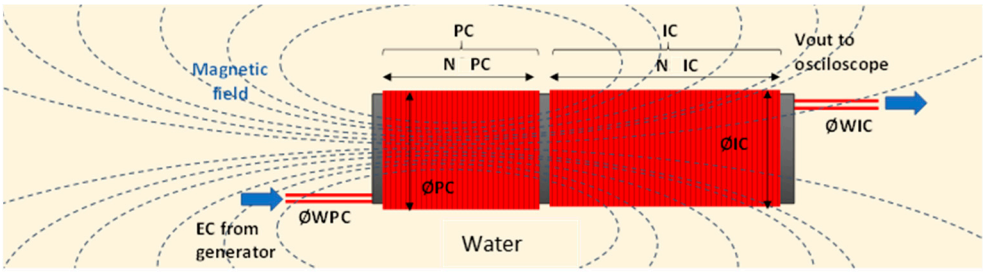

Figure 1. Presentation of the operation and variables of an induction coil in an aqueous medium.

This type of sensor has been revealed as a suitable sensor for monitoring water conductivity. In previous papers [26], it was demonstrated that the variation of different parameters, such as NS (Number of Spires), ØW, and ØIC or ØPC is vital to find the correct configuration of coils to sense a specific parameter. In this case, the parameter will be the amount of fertiliser in the water. As said before, μ_0 μ_r are modified by the conductivity of water.

2.1.2. Monitoring Parameters with Inductive Coils

On the other side, we can find the use of inductive sensors to obtain environmental data reported in several scientific articles. These inductive sensors are based on the creation of magnetic fields, which interact with the near environment, producing changes in the generated current. Wood et al. [28] developed, in 2010, a system that can measure water salinity based on inductive coils. The proposed conductivity sensor is composed of two coils. One is the powered and the other the induced coil. Their proposal is a solenoidal sensor covered with 1-dodecanethiol for protecting of the corrosion. Then a temperature sensor is used to adjust the values of conductivity to salinity.

Another author, such as Parra et al. [29], developed a system based on two coils for monitoring the conductivity in aquifers. They studied different configurations of prototypes based on different criteria: changes in the number of spires maintaining the spires relationship; changes in the relation of spires; changes in the relation of spires; changes in the wire diameter; and changes in the coil diameter. The paper concludes that the best prototype is composed of 80 spires in the induced coil, and 40 spires in the PC, the used copper and coil diameter is 0.4 mm, and the Polyvinyl Chloride (PVC) tube 25 mm. In addition, Javier et al. [20] developed an inductive coil for monitoring the inorganic fertilisers in the irrigation water. This sensor creates an electromagnetic field that is sensitive to the conductivity changes. They use different samples between 0 g/L and 45 g/L. Finally, they concluded that the sensors have an excellent correlation with a low average error of 2.15%. Pham et al. [30] designed a salinity sensor system. The initial laboratory testing shows that the salinity sensor system is functional and can be used to display salinity data on a given map. Other authors, as Kleinberg et al. [25] proposed a non-contacting electrical conductivity sensor for remote, hostile environments. They developed an inductive sensor that uses a single turn transmitter and receiver loops to generate and detect eddy currents in the materials. The results showed that the mechanical design of the sensor makes it insensitive to temperature and pressure changes, and accelerations, impact, and abrasion. Therefore, it is operable in remote, hostile environments, such as deep boreholes

The use of coils to measure in other environments, such as soil, is also well-known. Sänket et al. [19] developed a low-cost nitrate detection soil sensor. This system is based on a combination of capacitive and inductive electromagnetic fields for monitoring the content in agricultural soil and contamination. The proposed system concludes that the developed sensor will be able to detect various elements of

contamination, and also an improved design of the sensor can be researched. These prototypes can be used as a tool for water source monitoring in the farm where the nitrate level should not exceed 10 mg/L. Meanwhile, M. Parra et al. [31] presented a low-cost moisture sensor-based on inductive coils. They tested the inductive coils in different sorts of soils. Besides, they powered the coil using a voltage of 10 peak-to-peak volts. The experiment concluded that the best sensors work in 229 kHz with a correlation model of 0.75. Furthermore, the inductive coils as soil moistures sense have been compared with capacitive sensors in [32]. In this comparative study, M. Parra et al. demonstrated that for a range of temperature from 1 to 20 °C, the temperature of soil has almost no effect on the Vout of inductive coils, which is an advantage front the capacitive sensor in which case the effect of temperature is notable.

In the aforementioned papers, the viability of using the inductive coils as sensing method has been demonstrated for monitoring different environmental variables, which modify on the permeability of the medium, such as conductivity in the water of soil moisture. Although with these coils, we do not directly measure the variable itself, we measure the changes of the μ_0 and μ_r. As there is a relation between μ_0 and μ_r and the variable (conductivity of water), we can use this sensing coils.

Therefore, we propose the design, calibration, and verification of a prototype to monitor the amount of OF in water based on inductive coils. The prototype is able to measure the changes in conductivity associated with the fertiliser concentration. The OF is composed of organic material that provides less conductivity than inorganic fertilisers, as used in [20]. This causes the increase of the challenge because we have to be able to improve the accuracy and sensitivity of the optimal function of the tested prototypes. In addition, this system supposes an advantage in the irrigation water quality monitoring because no physical sensor for measuring OF has been reported. Thus, the proposed prototype in this paper is the first system able to measure and quantify the amount of OF in water, which will be essential to prevent over-fertilisation and other possible damages to the environment once implemented in the fertigation systems.

3. Materials and Methods

In this section, the materials used to craft and test the inductive coils, as well as the methodology used in their calibration and verification, are described.

3.1. Description of the Prototypes and its Fabrication

The prototypes are fabricated using PVC being a bracket of the sensor. This material used was due to its resistance to the water, its null conductivity, and its robustness. The used element must have no conductivity, since the objective is to have coils without a magnetic core as we need that the environment acts as a core. We developed three different prototypes. To minimise the existence of difference in the parameters that affect the mutual inductance, all of these sensors were made with the same bracket. The used PVC consisted of 3 mm of thickness, 25 mm of external diameter, and 22 mm of internal diameter.

We selected a relation of spires based on the results of previous works [33], so that all three prototypes were composed of 40 spires in the PC and 80 spires in the IC. The copper wire used had a diameter of 0.4 mm. The three prototypes had the same number of spires but were distributed in a different number of layers, to test which ones performed better in detecting OF. In the model presented in Section 2, the effect of a single layer, or multilayer coils, are not described, it is essential to figure out the effect of the number of layers in the sensitivity of the coil. The used prototypes are displayed in Figure 2. Prototype 1 (P1) had been coiled in 8 layers, prototype 2 (P2) in 4 layers, and prototype 3 (P3) was coiled in 2 layers (see Table 1). Moreover, all of the prototypes were coiled in the same direction (clockwise direction) to maintain the coil characteristics as similar as possible.

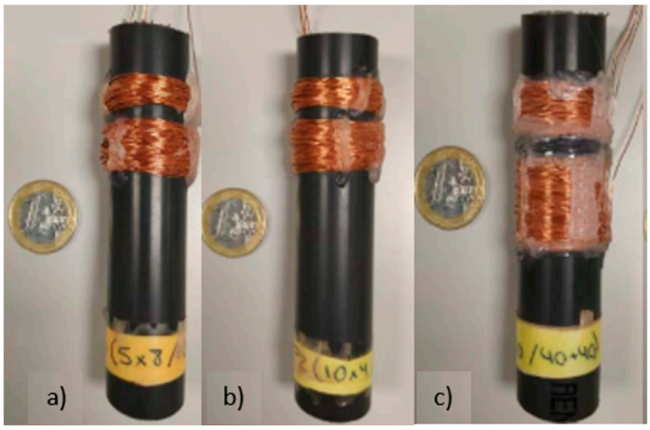

Figure 2. Representation of used prototype: (**a**) prototype 1 (P1)-40PC and 80IC (8 layers); (**b**) P2-40PC and 80IC (4 layers); (**c**) P3-40PC and 80IC (2 layers).

Table 1. Technical specification of the prototypes, with different number of layers.

Sensors	Prototype 1	Prototype 2	Prototype 3
Layers	8	4	2
Number of spires for layers	5/10	10/20	20/40
Longitude of the sensor (cm)	11.5	11	9.5

3.2. Methodology to Power the Coils

The prototypes were coiled in a clockwise direction, where the other end of the coil was used as a ground reference. The sensors were fed using a 3.3 Voltage peak to peak (Vpp). This paper offers new contributions as the evaluation of the effect of different electrical configurations, meaning, different modes of connections between the devices (generator and oscilloscope) and the coil in the Vout. Figure 3 portrays the implementation of four different configurations, where the polarity of feeding and measuring changed, and, therefore, the polarity of generated magnetic fields changed. The objective is to evaluate if the different configurations modified the Vout, and, if they did, which configuration provided the best results for the detection of OF. In the four cases, the modification in the connection changed how the magnetic field behaved, and how it interacted with the environment and with the IC.

3.3. Electromagnetic Effects on the Coils

In this section, the process used to perform the simulations prior to testing the sensors in a laboratory environment is described. As previously stated, COMSOL Multiphysics platform was used to model the proposed prototypes and simulate their behaviour in different mediums: air, pure water, seawater, and three different concentrations of OF. The values used to simulate the mediums in which the coils were immersed can be seen in Table 2. The values used to simulate seawater in COMSOL Multiphysics were chosen according to the results found in [34]. As for the values used to simulate the different samples of OF, we used the different conductivity values obtained during the experiments and a relative permittivity close to the one of pure water.

Table 2. Values used in the simulations.

	Air	Pure Water	Seawater	2.5 g/L of OF	12.5 g/L of OF	20 g/L of OF	Copper
Relative permeability	1	0.999992	1	1	1	1	1
Relative permittivity	1.00059	80	70	79.95	79.95	79.95	1
Conductivity (S/m)	0	5.5×10^{-6}	5.6	0.1133	0.415	0.614	5.998×10^{7}

In this paper, we will not be showing the simulations of the proposed prototypes in the different mediums. However, we decided to display the magnetic flux density and the electric field of all three prototypes using a 20 g/L of OF sample as a core, and explain the results obtained with COMSOL Multiphysics.

Figure 3 shows the magnetic flux density norm and the electric field of the prototypes using a 20 g/l of OF sample. Given the fact that the magnetic flux density highly depends on the permeability of the medium, and the relative permeability values used in the simulations are very similar, COMSOL Multiphysics did not manage to detect changes. The magnetic flux density norm values obtained during the simulations of P1 varied from 11.2 tesla (T) to 5.96 T along the edges of the induced coil, and from 11.2 T to 7.83 T along the centre of the induced coil (see Figure 3a). When the core was filled with air, the electric field of the prototype P1 varied from 148.36 V/m to 39.41 V/m along the edges of the induced coiled, and from 44.66 V/m to 17.91 V/m along the centre of the induced coil (see Figure 3b). In the case of pure water, the electric field varied from 247.28 V/m to 17.95 V/m along the edges of the induced coiled, and from 40.16 V/m to 13.74 V/m along the centre of the induced coil. For seawater, the obtained values of the electric field varied from 243.02 V/m to 87.81 V/m along the edges of the induced coiled, and from 40.33 V/m to 13.24 V/m along the centre of the induced coil. In samples of 2.5 g/L of OF, the electric field varied from 265.67 V/m to 14.11 V/m along the edges of the induced coiled, and from 40.03 V/m to 12.94 V/m along the centre of the induced coil. For the samples of 12.5 g/L of OF, the electric field varied from 267.36 V/m to 15.45 V/m along the edges of the induced coiled, and from 40.32 V/m to 13.14 V/m along the centre of the induced coil. Finally, the obtained values for the samples of 20 g/L of OF, the electric field varied from 268.86 V/m to 17.78 V/m along the edges of the induced coiled, and from 40.51 V/m to 13.35 V/m along the centre of the induced coil.

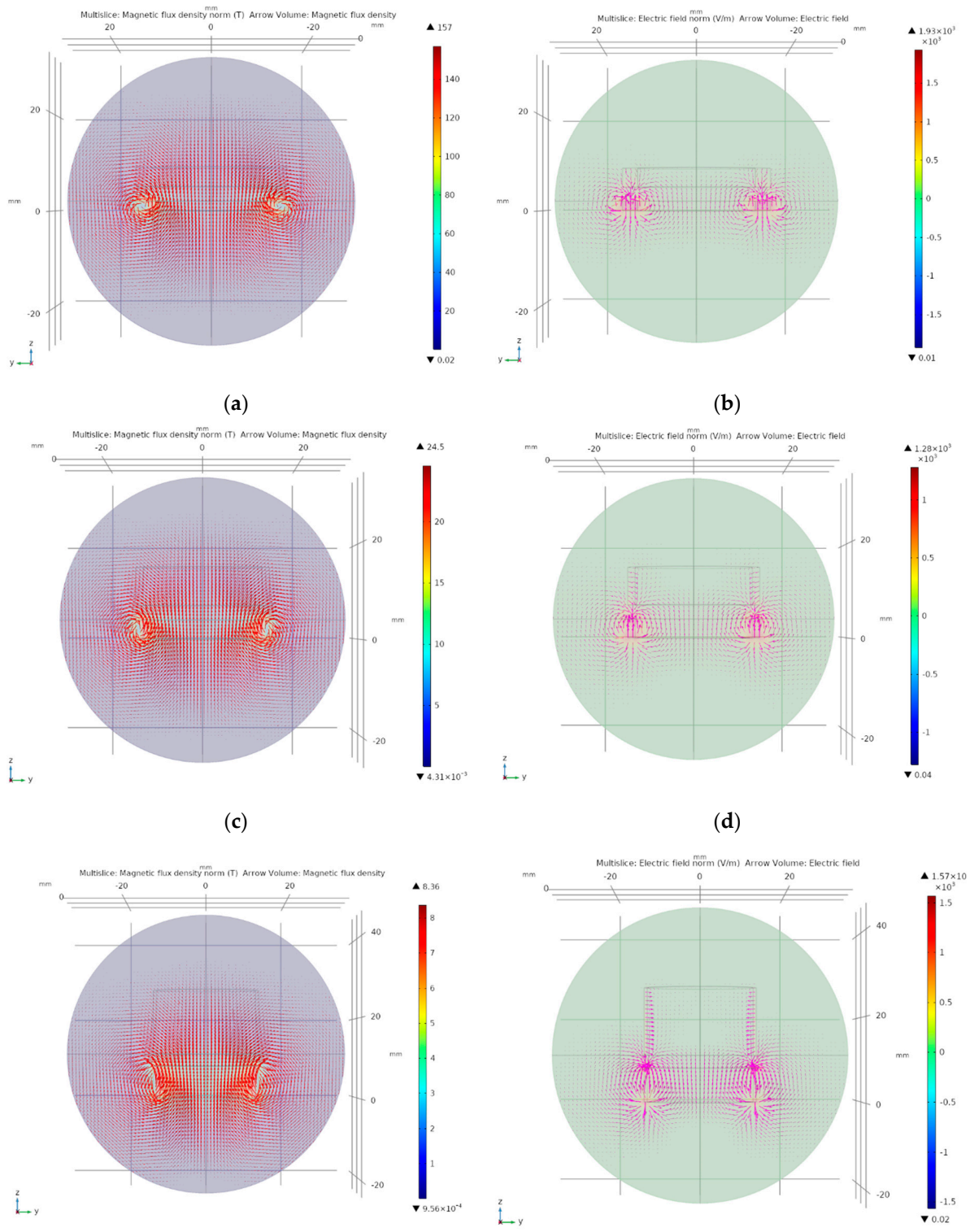

Figure 3. Simulations of the prototypes. (**a**) Magnetic flux density of P1 with 20 g/L of organic fertilizer (OF) sample. (**b**) Electric field of P1 with 20 g/L of OF sample. (**c**) Magnetic flux density of P2 with 20 g/L of OF sample. (**d**) Electric field of P2 with 20 g/L of OF sample. (**e**) Magnetic flux density of P3 with 20 g/L of OF sample. (**f**) Electric field of P3 with 20 g/L of OF sample.

Figure 3c,d display the magnetic flux density norm and the electric field of P2 using a 20 g/l of OF sample. In this case, the magnetic flux density norm values obtained varied from 5.29 T to 1.43 T

along the edges of the induced coil, and from 5.47 T to 2.18 T along the centre of the induced coil. For a core filled with air, the electric field varied from 132.67 V/m to 14.07 V/m along the edges of the induced coiled, and from 37.39 V/m to 0.73 V/m along the centre of the induced coil. In pure water, the electric field varied from 191.44 V/m to 11.2 V/m along the edges of the induced coiled, and from 36.52 V/m to 3.23 V/m along the centre of the induced coil. In seawater, the values of the electric field varied from 174.50 V/m to 19.65 V/m along the edges of the induced coiled, and from 36.43 V/m to 3.46 V/m along the centre of the induced coil. In the samples of 2.5 g/L of OF, the electric field varied from 190.72 V/m to 11.56 V/m along the edges of the induced coiled, and from 36.01 V/m to 3.35 V/m along the centre of the induced coil. In the case of samples of 12.5 g/L of OF, the electric field varied from 221.76 V/m to 12.63 V/m along the edges of the induced coiled, and from 36.13 V/m to 3.39 V/m along the centre of the induced coil. The obtained values for the samples of 20 g/L of OF, the electric field varied from 292.90 V/m to 21.6 V/m along the edges of the induced coiled, and from 36.41 V/m to 3.42 V/m along the centre of the induced coil.

Figure 3e,f present the magnetic flux density norm and the electric field of P3 using a 20 g/L of OF sample. The magnetic flux density norm values obtained varied from 2.20 T to 0.23 T along the edges of the induced coil, and from 2.45 T to 0.32 T along the centre of the induced coil. In the case of air, the electric field varied from 103.46 V/m to 5.43 V/m along the edges of the induced coiled, and from 25.25 V/m to 5.47 V/m along the centre of the induced coil. For pure water, the obtained values of the electric field varied from 158.98 V/m to 16.32 V/m along the edges of the induced coiled, and from 26.86 V/m to 8.8 V/m along the centre of the induced coil. In the case of seawater, the electric field varied from 251.89 V/m to 21.14 V/m along the edges of the induced coiled, and from 27.25 V/m to 8.76 V/m along the centre of the induced coil. For the samples of 2.5 g/L of OF, the values of the electric field varied from 230.48 V/m to 35.65 V/m along the edges of the induced coiled, and from 26.95 V/m to 8.85 V/m along the centre of the induced coil. In samples of 12.5 g/l of OF, the electric field varied from 257.77 V/m to 37.03 V/m along the edges of the induced coiled, and from 27 V/m to 11.19 V/m along the centre of the induced coil. Finally, for samples of 20 g/l of OF, the values of the electric field varied from 259.05 V/m to 39.62 V/m along the edges of the induced coiled, and from 27.05 V/m to 13.24 V/m along the centre of the induced coil.

3.4. Instrumentation

The used electrical circuit for this experiment is straightforward and easy to apply; it is represented in Figure 4. The circuit is based on the circuit used in previous papers [20] in which the coils are used as a sensing element. Firstly, we included a resistance of 47 ohms in serial in the PC. Moreover, a capacitator is added to 10 nF in parallel in the part of the IC. The sensor was powered with a signal generator, the AFG1022 [35]. The Vout was measured using an oscilloscope, the TBS1104 [36].

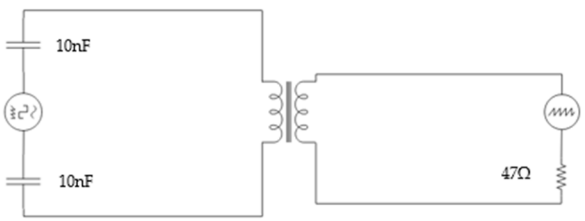

Figure 4. Diagram of the electronic circuit used in the experiment.

To control the conductivity of the samples and ensure that the relation between OF and conductivity is constant, a conductivity meter, the Basic 30 [37], is used. This device was calibrated before starting the conductivity measurements.

3.5. Equipment to Prepare the Samples

The experiments are performed using a glass container with 16.2 cm height and 8 cm of diameter, in which we introduce 500 mL of the sample. For the calibration, we use six samples between the 0 g/L and 20 g/L of OF, and the other three are used for the verification process.

As OF, we selected commercial produce, mainly used for citric crops as orange tree or lemon tree crops [38], which can be found in several specialised shops. We have chosen a semiliquid fertiliser to perform the experiment, due to its fast dilution in water. The selected product is called "ORGANIC" (trade name), and it was acquired in the garden section of Leroy Merlin. The selected OF is an organic-mineral fertiliser NK 3.5, which has 3% of organic nitrogen (N) of beetroot, 5% of potassium oxide (soluble in water), and 24.7% of organic carbon (C). The density of this product is approximately 1.3 g/cm^3 at 20 °C. Before starting the calibration, we prepared the samples and measured their conductivity with the Basic 30 to verify the correlation, 1 to 1, between both OF concentration and conductivity. This correlation is shown in Figure 5.

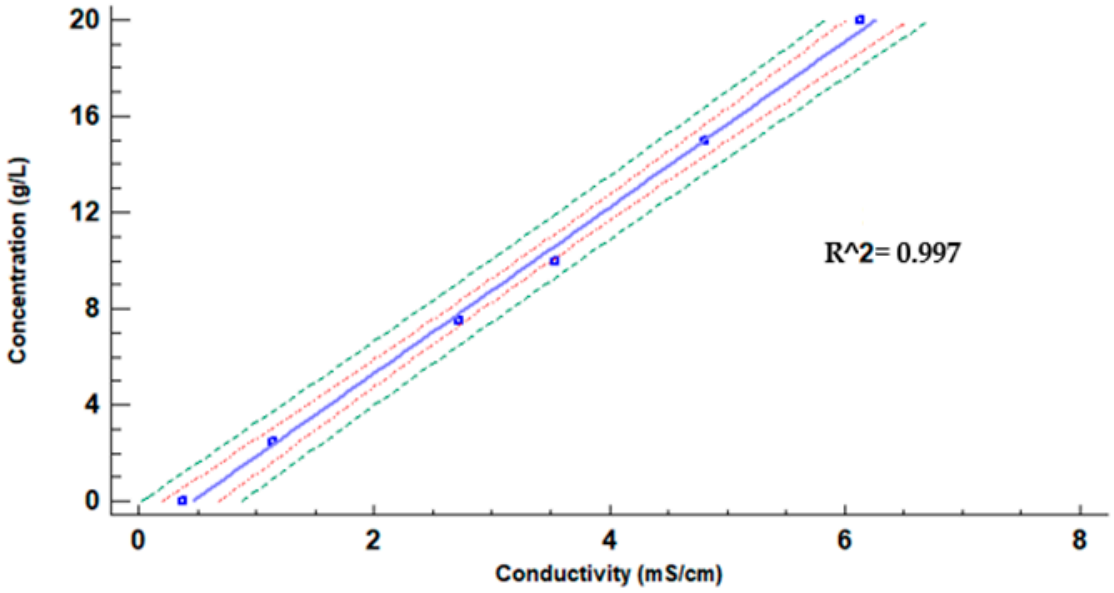

Figure 5. Tight model for OF concentration (g/L) vs. conductivity (mS/cm).

Following, we prepared the samples by mixing different amounts of the OF with the 500 mL of water to obtain the different concentration of the fertiliser, see Table 3. Some of the samples were used for the calibration process (CalPr) and others for the verification process (VerPr).

Table 3. The concentration of OF in the experiment. Calibration process (CalPr) and Verification process (VerPr).

Sample	**1**	**2**	**3**	**4**	**5**	**6**	**7**	**8**	**9**
OF (g/l)	0	2.5	5	7.5	10	12.5	15	17.5	20
Used for:	CalPr		VerPr	CalPr		VerPr	CalPr	VerPr	CalPr

3.6. Methodology to Conduct the Measures

Firstly, we performed a fast sweep between the 10 kHz and 300 kHz in each prototype for all the configurations, to find the region in which the Vout was highest. Based on the results of previous experiments, the WF was found in the region with the maximum Vout. To find the WF, we used six samples for the calibration. We calibrated the prototypes using six samples, see Table 3. The measures of Vout were replicated three times for each prototype and configuration in order to discard any

interferences. In addition, during each measurement, three values of Vout were gathered. The data used for the calibration represented the average value of Vout and the concentration of OF in g/L of each sample.

The process to have the calibration was performed as follows. Initially, we essayed with the four prototypes, testing each one in a specific spectrum of frequency, from 10 to 300 kHz, to find the WF. It was done considering the four configurations of each prototype, as indicated in Figure 6. After analysing the range of frequency, where the P1, P2, and P3 were more affected by the concentration changes, we chose the WF for each prototype in the four studied configurations. Furthermore, we used the Vout values in the WF to obtain a mathematical model for the tested prototypes to verify which equation adjusted better to obtain data. To get this, we used specific software, Statgraphics [39], which is very useful for analysing the values.

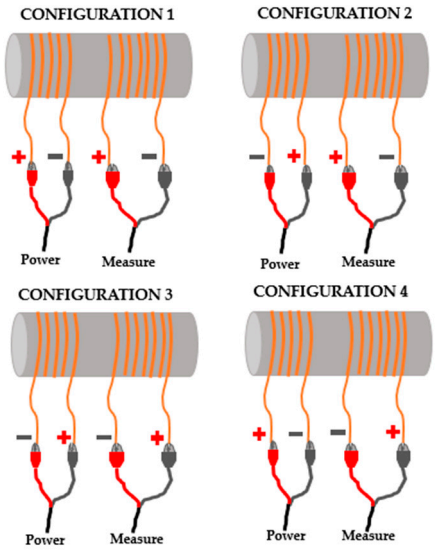

Figure 6. Different modes and configurations to measure *Vout,* tested in calibration and verification.

Once the calibration test finished and calibration models were obtained, we used the other three samples (5 g/L, 12.5 g/L, and 17.5 g/L) to verify the calibrations and their mathematical models. With the data of verification, we calculated the Absolute Error (AE) and Relative Error (RE) between the real concentration of OF and predicted OF concentration based on measured Vout and the calibration models for the tested samples.

Finally, we applied the ANOVA [40,41] procedure to verify if the obtained data were relevant. Likewise, we used the multiple range procedure to determine if the different concentrations of OF explained the variance of the variable Vout. We use the Least Significant Difference Turkey (LSD Tukey) method for significant differences between pairs of means for the comparisons among the concentrations of fertilizer. In this case, we obtained two indicators, Reason-F and Value-P. The former is used to determine whether, from among a group of independent variables, at least one has the ability to explain a significant part of the variation of the dependent variable. Moreover, Value-*P* is useful to know if the obtained results are the consequence of random sampling, or if they are statistically significant. This procedure is used to choose which prototype is the best one, in terms of its capability to differentiate the samples, to be selected as a sensor for measuring OF. Subsequently, we analyse the data for all cases in the three prototypes, using a single ANOVA operation to obtain the relevance of the measured values, and we evaluated the standard deviations of the prototypes for each configuration. Finally, we selected the best prototypes based on previous results.

Since, in past experiences, we detected different behaviours of inductive coils, we set a series of requirements that prototypes must accomplish in order to be selected as a capable sensor. Those requirements are described below:

a. The difference of Vout between the samples of OF must be as high (at least a variation of 1 V between the less concentrated sample and the more concentrated sample).
b. The measured Vout must be as higher as possible (at least 3 V).
c. The Vout for all tested samples must be different (variations lower than 0.001 V are not considered as different values).
d. The working frequency must be as low as possible (the maximum allowed frequency will be 200 kHz).
e. The AE and RE must be low (AE must be lower than 1.5 g/l in the lowest verified concentration and RE lower than 10% as the average for all samples).

4. Results

The acquired results for the different samples are exposed in this section, including the calibration, verifications, and statistical tests.

4.1. Calibration

In this subsection, the data gathered for the seeking of the WF and the calibration of the three prototypes is presented. To select the WF, we sought the frequency among the samples, ones in which the difference of Vout, between the most and the less concentrated samples, is maximised.

For the first prototype, the highest values of Vout, higher than 3 V, as indicated in the requirements, we registered between 80 kHz and 110 kHz, see Figure 7. In this frame, Figure 7 represents that, in all the configurations, the maximum Vout, 9.65 V, is measured when the PC is fed at 100 kHz. Additionally, Table 4 displayed the maximum difference between the Vout of 0 g/L and 17.5 g/L. The maximum difference is found at the frequency of 90 kHz in three out of four tested configurations, and 100 kHz for the other one. The values of WF for the P1 show a growing tendency, for all of the tested configurations, being the minimum Vout for 0 g/L and the maximum measured voltage for 17.5 g/L. This shows that the different configuration to feed the coil may affect the obtained values, as a low modification of the WF.

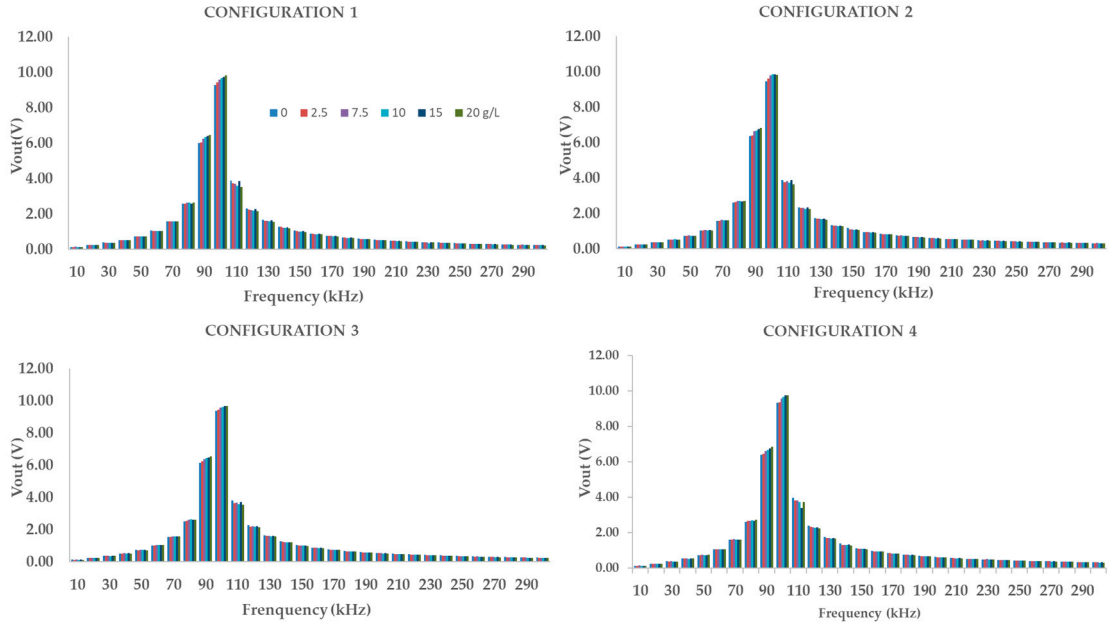

Figure 7. Representation of the frequency spectrum of P1 in the four different studied cases.

Table 4. Frequency and Vout difference for P1, P2, and P3 and their four configurations (Conf.).

Prototypes	Conf. 1	Conf. 2	Conf. 3	Conf. 4
	PF (kHz) among the sampled frequencies			
P1	100			
P2	120			
P3	140			
	WF (kHz) among the sampled frequencies			
P1	100	90	90	90
P2	110	110	110	110
P3	140	140	140	130
	Difference in *Vout* Sample 8—Sample 1			
P1	0.53	0.44	0.39	0.43
P2	1.07	1.41	1.41	1.84
P3	−1.29	−1.15	−1.47	1.09

In the case of configurations 2 to 4, the differences in Vout of calibration tests are almost the same, 0.44, 0.39, and 0.43. Considering that standard deviations for those values are 0.028, we can affirm that no differences are found. Although the differences in Vout between most diluted and most concentrated samples is almost constant, the Vout values for the tested values are different. The results are similar for configurations 2 and 4, and different for configuration 3. For configurations 2 and 4, the mean Vout for the most diluted sample is 6.37 V and 6.40 V, and 6.81 V and 6.83 V for the most concentrated sample. On the other hand, for the third configuration, the values are 6.15 for the most diluted sample, and 6.53 V for the most concentrated sample. These small changes suppose a difference in the Vout of almost 0.2 V between the same samples measured with different configurations. With regards to configuration 1, the difference on the Vout is the highest, 0.53, and the difference between the maximum (9.81) and minimum (9.28) Vout measured with this configuration and the rest are even higher, up to 3 V.

Concerning the second prototype, Figure 8 shows the gathered data for the calibration at different frequencies. According to the data, we can identify the most potent interaction between the Vout and the sample and with Vout higher than 3 V between the 100 kHz and 140 kHz. In this range, the highest values are located at the peak, 110 kHz in all the analysed configurations. In this frequency, the registered highest Vout is around 9.81 V. The P2 offered higher Vout values when the concentration of OF increased, as with P1. This observation indicates a similar functioning between the two prototypes. Table 4 represents the highest difference of Vout between the lowest concentration sample and the most concentration. Moreover, the measures of the different tests that we did with P2 indicate that the highest voltage difference is found in configuration 4, with 1.84 V.

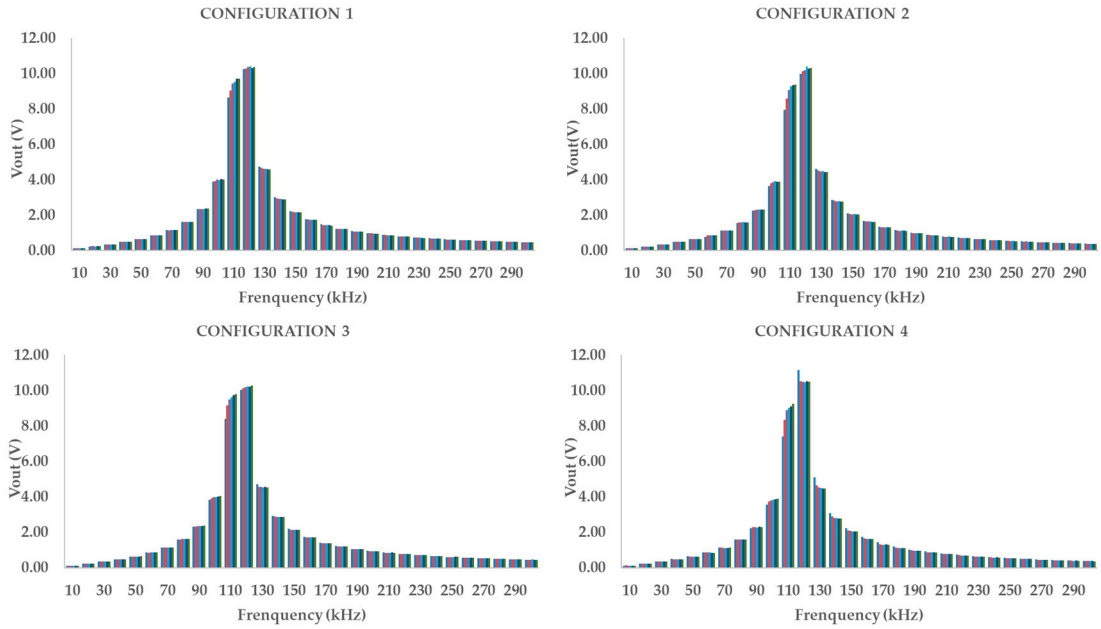

Figure 8. Representation of the frequency spectrum of P2 in the four different studied cases.

Concerning the variability between tested configurations, P2 has high variation in the differences between maximum and minimum concentrations of OF in the WF. While in the first configuration the difference between most diluted and less diluted sample is 1.07 V, in the case of configuration 4, this value reaches the 1.84 V. In the second and third configuration, the difference is 1.41 V. With regards to the Vout values in the samples, configuration 4 is the one with the lowest voltage in the most diluted concentration (7.41 V). On the contrary, configuration 1 reached a Vout of 8.64 V for the same sample. This change on Vout, a higher value for the first configuration, is maintained along with all of the tested samples. So that, a variation of more than 1 V is observed for the same prototype, sample, and WK if the configuration is modified in the lowest.

For the third prototype, the results are represented in Figure 9. For this prototype, ranges with Vout higher than 3 V cover between 130 kHz and 150 kHz. In this case, the highest Vout that we registered is the smallest one among the three prototypes, 6.35 V. P3 shows that the voltage peak is located in a higher range of frequency than in other prototypes. Table 4 shows the highest difference of Vout between the minimum and maximum concentration of OF. The maximum difference is found at 140 kHz in three out of four configurations and 130 for the other, as found with P1. Notwithstanding what we detected in P1 and P2, the data of P4 shows the maximum Vout for the less concentrated sample, in three out of four configurations. The maximum difference between higher and lower Vout is detected in the configuration 3, with –1.47 V.

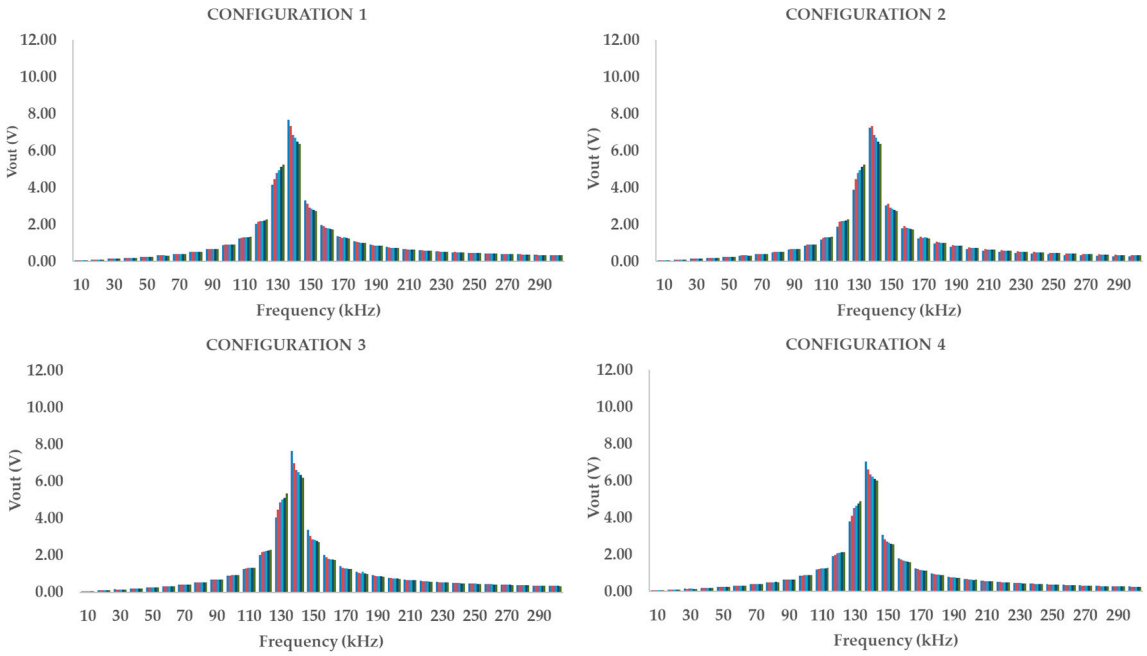

Figure 9. Representation of the frequency spectrum of P3 in the four different studied cases.

With regard to configurations 1 to 3, which share the same WF, the difference among the lowest and highest concentrations are 1.29, 1.15, and 1.47 V respectively. Meanwhile, configuration 4, characterised by the lowest WK, has a variation in the measured Vout of −1.09 V, which is lower than the variation for other configurations. If we analyse in detail, the different maximum and minimum values, not only the differences between them, configurations 1 and 3 have a similar pattern. Both configurations have similar values, 7.65 V for configuration 1 and 7.65 V for configuration 3 in the case of the less concentrated sample. Meanwhile, for configuration 2, the Vout is 7.23 V for the same sample, a variation on nearly 0.4 V is found. It has no sense to compare the differences with the results with the fourth configuration since the last configuration is characterised by a behaviour similar to the one found in P1.

All of the evaluated prototypes presented a similar range in which their respective Vout is affected by the concentration of tested samples. At these frequencies, their WF, we obtain higher Vout values and higher Vout differences. This range is located between the 90 k kHz and 140 kHz. The next step is to obtain the mathematical model that fits with the data gathered for the calibration at the WF for each prototype and their four configurations.

The obtained calibration models for all configurations of P1 are presented in Figure 10. Among the 27 possible models available in Statgraphics, the one that offered the best adjustment, in terms of Coefficient of determination (R2), is the lineal model for all the configurations of P1. This model has the advantage of its low complexity. The values of R2 are indicated in Figure 10, and they have a minimum value of 0.937 for configuration 2. Configuration 4 is the one that presents the best adjustment between the mathematical model and gathered data with R2 of 0.995. With regard to the mathematical models, they are represented in Equations (9) to (12) for each one of the configurations of P1. These equations will be included in the node when the sensor will be part of a WSN to convert the measured electric signal into the value of the sensed parameter. Their confidence and prediction intervals are displayed in Figure 10.

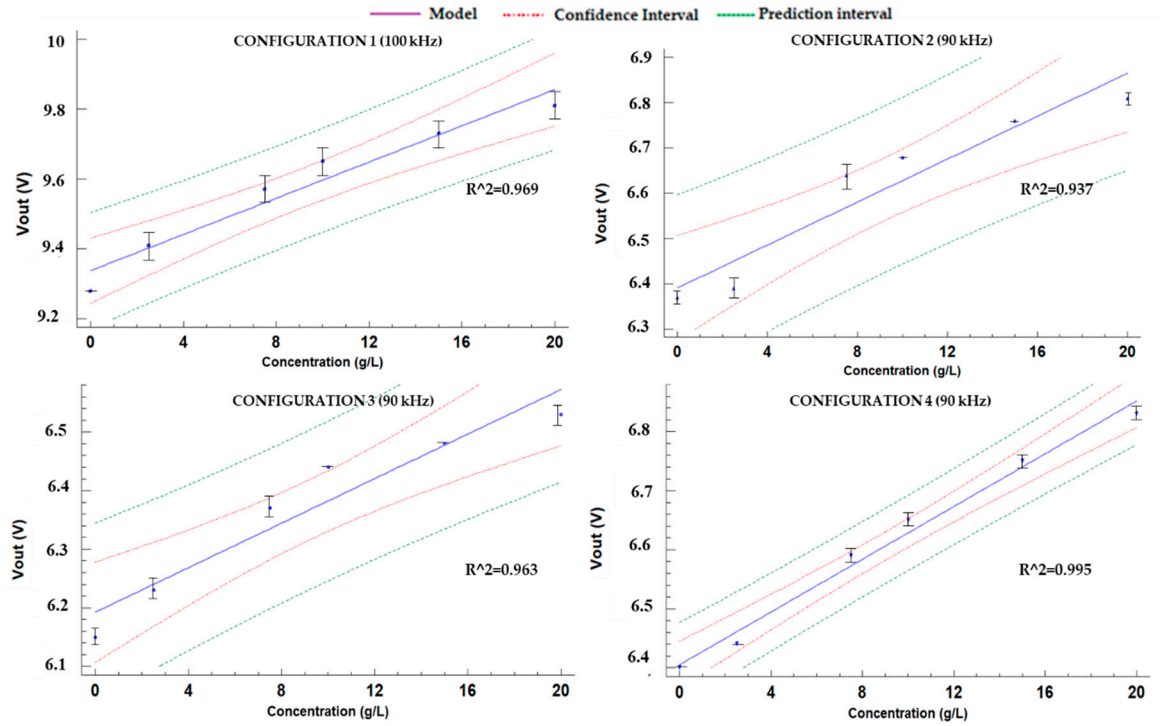

Figure 10. Adjusted models of P1.

$$Concentration\ (g/L) = -343{,}014 + 367{,}813 * Vout(V) \quad (9)$$

$$Concentration\ (g/L) = -24{,}551 + 385{,}388 * Vout(V) \quad (10)$$

$$Concentration\ (g/L) = -300{,}911 + 487{,}033 * Vout(V) \quad (11)$$

$$Concentration\ (g/L) = -283{,}199 + 442{,}308 * Vout(V) \quad (12)$$

On the other hand, calibration models for the configurations of P2 are shown in Figure 11. The values of R2 are included in Figure 11. Configuration 3 presents the lowest R2, with a value of 0.980. On the contrary, the best adjustment between the mathematical model and gathered data is found in configuration 1, with R2 of 0.995. The mathematical models are detailed in Equations (13)–(16) for each one of the configurations of P2. Their confidence and prediction intervals are displayed in Figure 11. In general terms, the R2 values of mathematical models obtained for prototype 2 are better than the R2 of models generated for prototype 1.

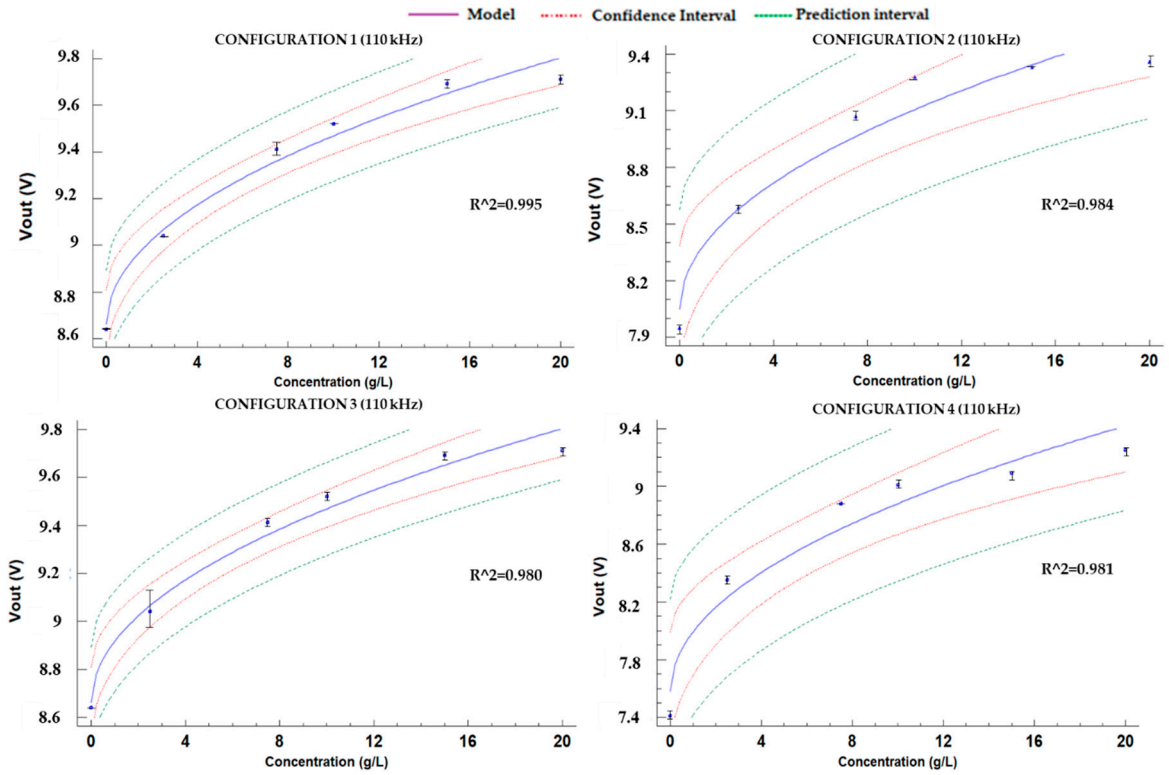

Figure 11. Adjusted models for the P2.

Finally, Figure 12 displays the calibration models for all configurations of P3. The calibration model with the lowest R2 has a value of 0.970, and it is linked to the data of configuration 1. Configuration 2 has the best adjustment with an R2 of 0.997. The mathematical models are represented in Equations (17)–(20) for each one of the configurations of P2. The models that correlated the data of prototype 3 are the ones with better R2 values.

$$Concentration\ (g/L) = (373{,}299 - 323{,}289/Vout(V))\text{^}2 \quad (13)$$

$$Concentration\ (g/L) = (262{,}884 - 210{,}467/Vout(V))\text{^}2 \quad (14)$$

$$Concentration\ (g/L) = (288{,}277 - 244{,}709/Vout(V))\text{^}2 \quad (15)$$

$$Concentration\ (g/L) = (206{,}431 - 155{,}121/Vout(V))\text{^}2 \quad (16)$$

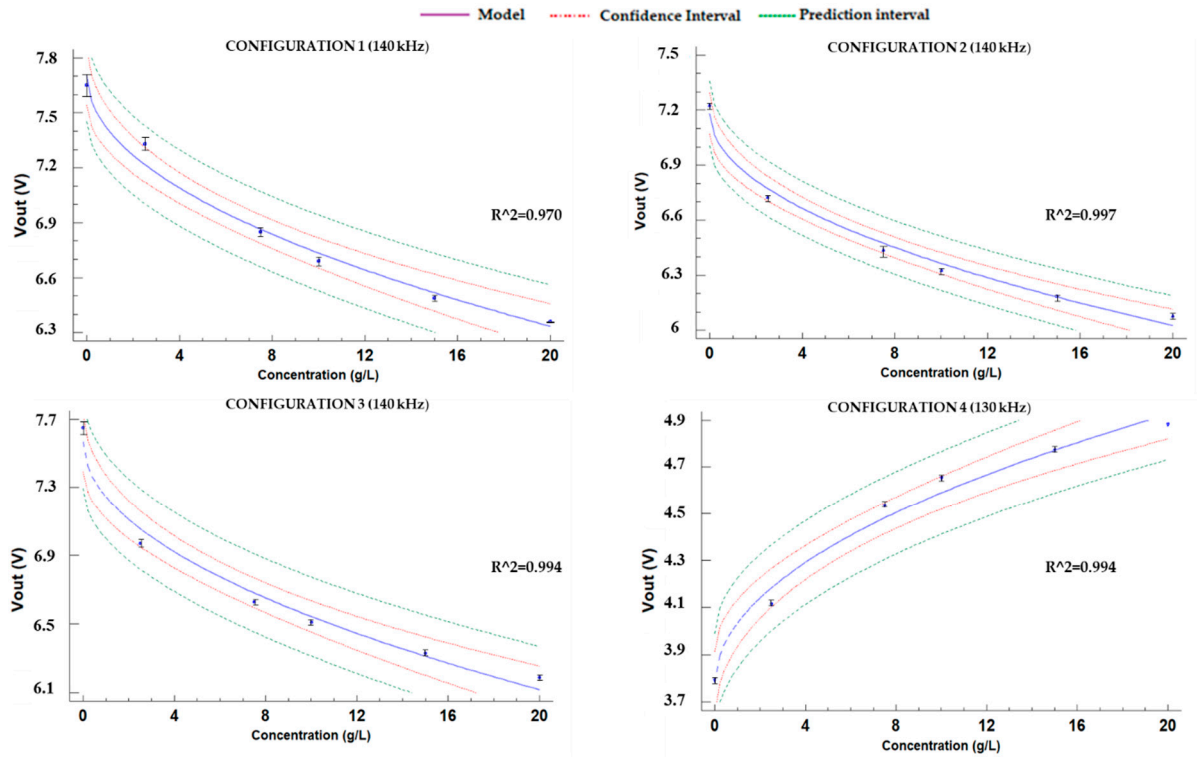

Figure 12. Adjusted models for P3.

$$Concentration\ (g/L)\ = (-202{,}107\ +\ 156{,}869/Vout(V))\text{^}2 \quad (17)$$

$$Concentration\ (g/L) = \ (-23{,}558\ +\ 169{,}702/Vout(V))\text{^}2 \quad (18)$$

$$Concentration\ (g/L) = \ (-19{,}118\ +\ 145{,}337/Vout(V))\text{^}2 \quad (19)$$

$$Concentration\ (g/L) = \ (186{,}403\ -\ 707{,}278/Vout(V))\text{^}2 \quad (20)$$

4.2. Verification

In this subsection, the results of the verification test are analysed. Table 5 displays the results in terms of AE and RE for all the samples measured in the verification test, with all the prototypes and configurations. The AE and RE are calculated using absolute values (being all obtained results positive).

Table 5. Verification of the calibrations of the prototypes. Abbreviations: Absolute Error (AE) and Relative Error (RE).

Concentration of OF (g/L)	Conf.	P1		P2		P3	
		AE (g/l)	RE (%)	AE (g/l)	RE (%)	AE (g/l)	RE (%)
5.00	1	1.04	20,81	0.66	13.26	0.02	0.43
12.50		2.37	18,94	0.85	6.81	0.41	3.3
17.50		0.31	1,77	2.04	11.64	0.02	0.12
5.00	2	0.78	15,57	2.11	42.25	1.71	34.1
12.50		0.97	7,77	0.52	4.19	1.05	8.43
17.50		2.49	14,22	3.04	17.37	1.06	6.03
5.00	3	1.41	28,14	2.66	53.14	0.52	10.43
12.50		1.70	13,59	1.03	8.21	0.84	6.71
17.50		1.35	7,73	2.42	13.85	2.46	14.05
5.00	4	1.14	22,82	3.15	62.91	0.85	16.97
12.50		1.53	12,26	0.03	0.28	0.55	4.44
17.50		0.37	2,12	3.61	20.63	1.28	7.33
Average error	1	1.24	13,84	1.18	10.57	0.15	1.28

2	1.41	12,52	1.89	21.27	1.27	16.22
3	1.49	16,49	2.04	25.06	1.27	10.40
4	011.	12,40	2.26	27.94	0.90	9.58

The average AEs, considering all samples for each prototype and each configuration are lower than 2.3 g/L in all the cases. The highest average AE is detected for the P2 and the fourth configuration. In general terms, we can affirm that P2 is the ones with higher AEs with average AE of 1.18 g/L for configuration 1, as the lowest AE, and 2.26 g/L for configuration 4, as the highest AE. According to results of P1, its AEs are lower than the ones of P4, being the configuration 4 the one with lowest AE (1.01 g/L) and configuration 3 the one with the highest AE (1.49 g/L). Finally, data from P3 is characterised by low AE; the minimum and maximum average AEs are 0.15 g/L for configuration 1 and 1.27 g/L for configurations 2 and 3. Thus, in general terms, P3, and particularly the first configuration, is the combinations which offer the lowest average AE in the verification tests.

According to the AE in the less concentrated sample, which was one of the requirements for our sensor, the lowest AE is obtained for P3 and first configuration (AE of 0.02 g/L). The data of P2 in verification tests is again the one with highest AE. There are only five combinations of prototype and configurations which ensure an AE in the less concentrated sample lower than 1 g/L: P1 configuration 2, P2 configuration 1, and P3 configurations 1, 3, and 4. We have not detected that the AE increases or decreases with the concentration of the verified sample.

The RE is highest in the verification sample with less concentration of OF in most of the cases. Attending to the differences between the prototypes and their configurations, we can see in Table 5 that the P1 is the one with more stable RE, as happened in AE. P2 is the one with the highest RE, and P3 is characterised by the smallest average RE.

4.3. Statistical Analysis

Finally, the results of statistical tests aimed to evaluate the reliability of our data are presented. The results of the multiple range tests to show the number of groups created according to the data of CalPr and VerPr are described. For all of the evaluated data (all prototypes and their four configurations) the results of ANOVA indicate that the concentration of OF explains the variance on the Vout.

Figure 13 represents the output of multiple range tests for each configuration of P1. Among these four configurations, the best results are obtained for the configurations 3 and 4. In these configurations, we find the highest differentiation in terms of generated groups. For configuration 3, the results of the test define nine groups (a to i), and for the fourth configuration eight groups (a to h) are defined. Each column of letters indicates a group of means within which there are no statistically significant differences. The first and the second configurations are very similar, and only seven groups can be identified (a to g). With data of the first configuration, it is not possible to distinguish between 12.5 and 15 g/L or between 17.5 and 20 mg/L. In the case of the second configuration, the lack of differentiation is found between 0 and 2.5 g/L and between 15 and 17.5 g/L. The standard deviation of the configurations is very low, being 0.041 g/L, 0.012 g/L, 0.018 g/L and 0.015 g/L for configurations 1 to 4 respectively.

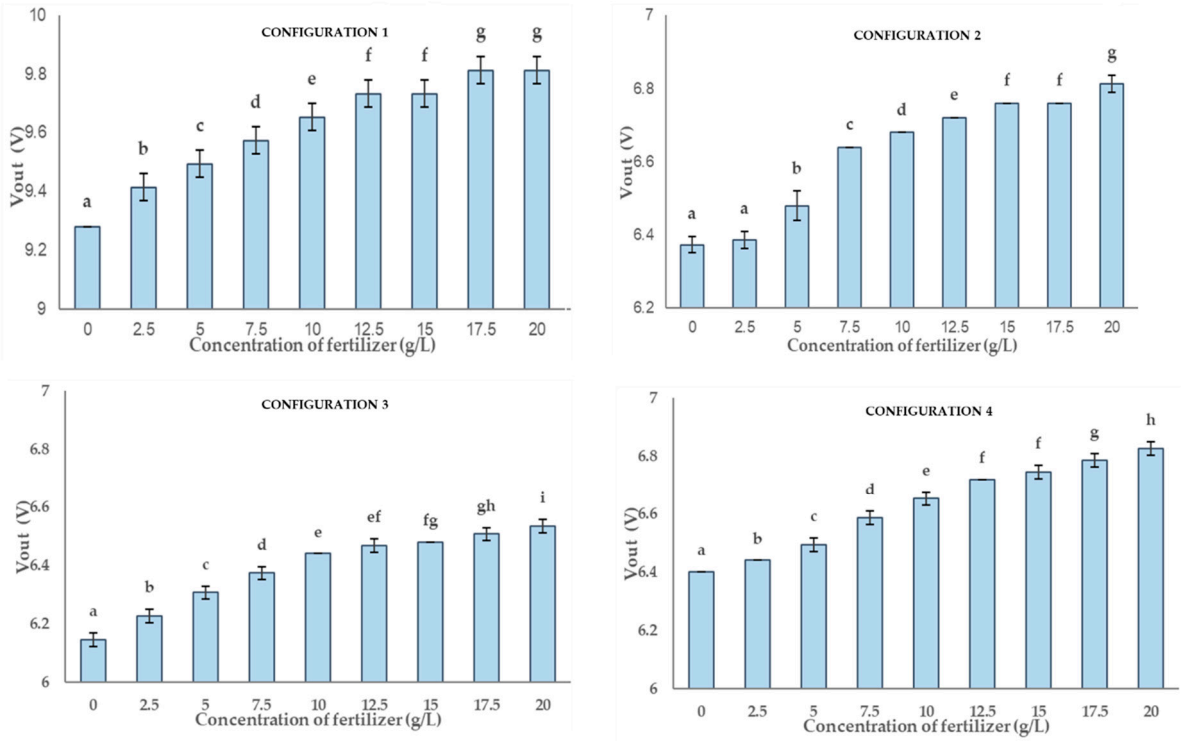

Figure 13. The graph presents a multi-range analysis for the four configurations where they are drawn by columns. Each column contains non-significant values between them. The different letters show that the values are statistically significant. In each column the vertical bar on it represents the standard deviation.

Following, the results of P2 are displayed in Figure 14. The best results are related to the data gathered from configuration 1, followed by configuration 2 and 3. In this context, the results of statistical tests identify for configuration 1 has 8 different groups (a to h), and six groups (a to f) for configuration 2 and 3. Data from configuration 4 have been organised in six groups (a to f), as configuration 2 and 3. Nonetheless, data is more homogeneous, especially in the case of more concentrated samples. Thus, it is not possible to distinguish 17.5 g/L and 20 g/L and hard to distinguish between 10 g/L to 15 g/L. The standard deviations of all configurations are very low. The lowest standard deviation is found for configuration 1 with 0.018 g/L, followed by configuration 2 with 0.03 g/L. Configuration 3 and 4 are the cases with the highest standard deviation, 0.06 g/L and 0.04 g/L, respectively. In this case, the results point out that P1 has a lower deviation standard than P2. Furthermore, P1 is characterised by a higher number of groups in their configuration than P2.

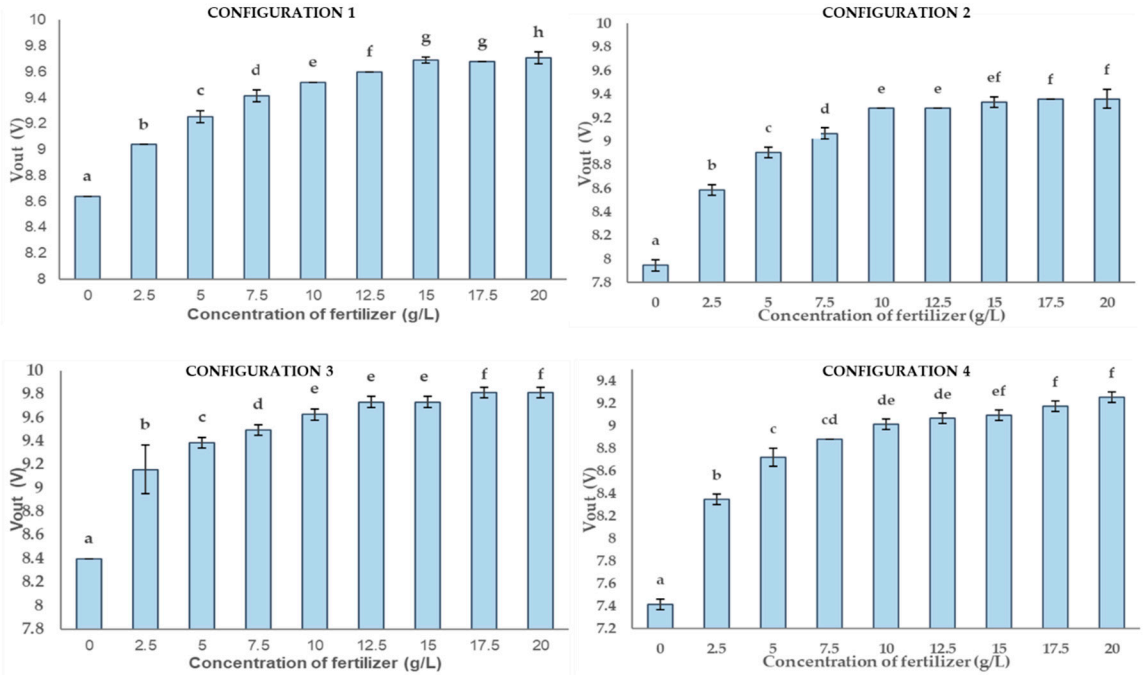

Figure 14. The graph presents a multi-range analysis for the four configurations where they are drawn by columns. Each column contains non-significant values between them. The different letters show that the values are statistically significant. In each column, the vertical bar on it represents the deviation.

Figure 15 displays the results of the multiple range test for the four different configurations of P3. The best results are obtained for configurations 1 and 4. The data of both configurations are distributed in nine different groups (a to i). For configuration 2, we can identify seven groups (a to g). For configuration 2, the values of 0 g/L and 2.5 g/L, and 5 g/L and 7.5 g/L are the same. Meanwhile, eight groups (a to h) are formed with data of configuration 3. The standard deviation of this prototype is very low, lower than in other prototypes. The lowest values are obtained with data of configuration 4, 0.02 g/L. The highest standard deviation is linked to data of configuration 1, 0.03 g/L. Comparing the number of groups and their standard deviations, we can affirm that P3 is the prototype with better results.

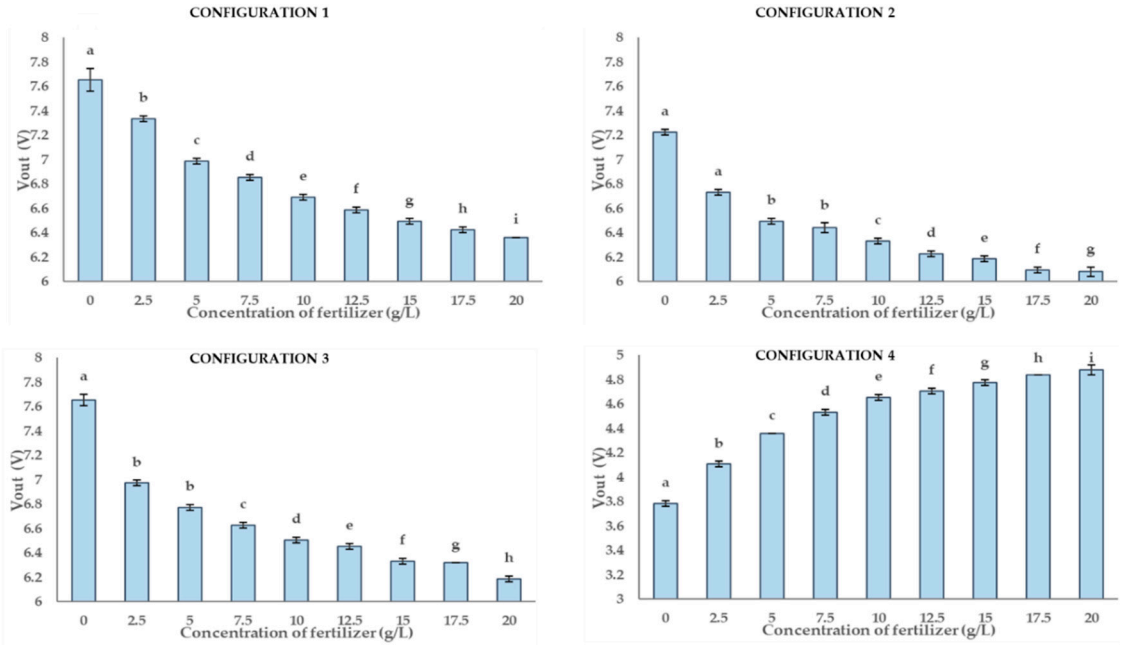

Figure 15. The graph presents a multi-range analysis for the four configurations where they are drawn by columns. Each column contains non-significant values between them. The different letters show that the values are statistically significant. In each column the vertical bar on it represents the deviation.

5. Discussion

5.1. Differences Observed Among the Four Tested Configurations

One of the most significant findings of the performed tests is the comparison of the four configurations. Although the generated magnetic field should be uniform no matter the polarity of the coil, as some of our inductive coils are composed by a high number of layers, and they are manually crafted, it is necessary to evaluate this effect.

The first difference was observed during the calibration tests, in which two prototypes have shown different WF when the configuration is changed. In P1, the WF was higher with the first configuration. Meanwhile, for P3, the lowest PF was measured in the fourth configuration. Since the test is performed three times, and in all the cases, the results were the same, the observed change in WF due to the different configuration parameters must be considered in future prototypes. More tests needs to be done to find the exact WK, since we measure every 10 kHz to have more information about this effect. Notwithstanding the aforementioned (about the WF), the PK is found at the same frequency among the sampled ones. As with the WF, more data is needed to evaluate that the different configuration patterns might modify the PK.

The other parameter, which was modified due to the different configurations, is the Vout. We are going to evaluate the changes in Vout of P1 with configurations 2 to 4, P2 in all the configurations, and P3 in configurations 1 to 3. The other two configurations are not considered since a difference in the WF is detected in the excluded configurations. We can affirm that the fact of change the configurations has caused a change in the Vout, which is not explained by the changes in the WF since all the comparisons are made with the same configuration. According to P2 and P3, the Vout values in configuration 1 and 3 show an almost equivalent trend. The Vout of the first configuration is a bit higher in all of the samples than in the third configuration, an average a 0.17 V higher. The second and fourth configurations tend to have lower values than the previous ones.

This effect has been found in other publications related to inductive coils [29].

5.2. Decreasing and Increasing Vout with the Changes in Conductivity Before and After the PF

The change in the increaser of decreasing tendency of Vout for the increase of the concentration of OF is found in this paper. According to our data, in all of the tested prototypes and all of the studied configurations, the tendency is, the higher the concentration, the higher the Vout before the PF. Nonetheless, after the PF, the higher the concentration of OF the lower the Vout. This effect can make difficult the use of the prototype as a sensor and the attainment of calibration curves in the frequencies close to the PF. However, considering that the Vout is higher only in the frequencies close to the peak, we identify a trade-off in which both phenomena must be carefully considered in the selection of WF of inductive coils.

This effect, the change in the behaviour of Vout and concentration in inductive coils, has been already found in other applications of inductive coils as soil moisture sensors. In [32], a similar effect is detected when similar prototypes are tested for soil moisture monitoring. In that case, the Vout increases with the soil moisture before the PF and decreases after the PF. The same effect is observed in [32] when the inductive coils are studied as a soil moisture sensor in different types of soil.

5.3. The Best Prototype to be Used and OF Sensor in PA Systems

These prototypes are the best sensors tested in previous studies [20]. Furthermore, these prototypes differ in the distribution of their layers. With this comparison, we will verify which

sensor, with which layer distribution, is the most suitable for monitoring OF. It also serves as a precedent for future research in the development of sensors for fertilizers.

After analysing all of the measures in calibration, verification, and statistical analysis, it is time to compare the prototypes and identify the one with the best performance. According to the requirements set in Section 3, we have five different requirements; all of them are analysed in Table 6. The first requirement is a minimum variation of 1 V between the most and less concentrated samples (ΔVout [S1–S9]). According to our data, only the P2 and P3 accomplish this requirement. The second requirement was related to the Vout magnitude, the lower registered Vout (Minimum. Vout*)* should be at least higher than 3 V. In this case, all of the prototypes fulfil this requisite. The third condition is that Vout must be different in all the samples. To test this requisite, we base on the results of a multiple range test. According to Table 6, this requisite is reached only in three cases, P1 configuration 3, P3 configurations 1 and 4. With regards to the working frequency (WF), all of the prototypes have WFs lower than the required threshold, so that they all are considered as valid. The last requisite refers to the error measured in the verification test, in this case, the AE for the lowest verified concentration (AE [S3]) and the average RE ($\overline{RE}$)must be considered.

Table 6. Statistical ANOVA test to analyse measured values. The requirements to be met by the prototypes are shown so that they are optimal for measuring OF, where "P" means prototype and "R" requirement. Values with an asterisk indicate that the requirements are met.

	Conf.	R1	R2	R3	R4	R5		All
		Δ*Vout* [S1–S9] (V)	**Min. *Vout* (V)**	**Nº Groups**	**WF (kH)**	**AE [S3] (V)**	**$\overline{RE}$ (%)**	
P1	1	0.53	9.28 *	7	100 *	0.02 *	0.19 *	
	2	0.44	6.37 *	7	90 *	0.03 *	0.52 *	
	3	0.39	6.15 *	9 *	90 *	0.22 *	3.5 *	
	4	0.43	6.40 *	8	90 *	0.07 *	1.05 *	
P2	1	1.41 *	8.64 *	8	110 *	0.65 *	7.05 *	
	2	1.41 *	7.95 *	6	110 *	0.75 *	8.45 *	
	3	1.41 *	8.40 *	6	110 *	0.7 *	7.41 *	
	4	1.84 *	7.41 *	6	110 *	0.83 *	9.53 *	
P3	1	1.29 *	7.65 *	9 *	140 *	0.62 *	8.86 *	*
	2	1.15 *	7.23 *	7	140 *	0.41 *	6.28 *	
	3	1.47 *	7.65 *	8	140 *	0.6 *	8.81 *	
	4	1.09 *	3.79 *	9 *	130 *	0.36 *	8.34 *	*

Analysing the results for each one of the tested prototypes and their four configurations, we only found two cases in which all the requirements are accomplished, P3 configurations 1 and 4. Among both configurations, P3-configuration 1 is characterised by higher ΔVout [S1–S9], higher Min. Vout, and lower AE [S3], although it has a higher WF than configuration 4. In the case of P1 configuration 1, ΔVout [S1–S9] is lower than 1, which does not meet one of the most important requirements. Therefore, after comparing the performance of each prototype, we selected P3 with the first configuration as the best prototype for its use as an inductive sensor for OF monitoring the fertigation in PA systems.

6. Conclusions

We evaluated the effectiveness of inductive coils as a sensor to measure the concentration of OF used in agriculture. The obtained parameters will be used to monitor the quantity of OF in the irrigation systems to detect abnormal situations or deficiencies.

In this paper, we showed the performance of three different prototypes with four configurations as a sensor to measure the concentration of OF. First of all, the performance of each prototype was analysed using COMSOL Multiphysics, and the WF of each prototype and configuration is determined after testing the sensor in a laboratory environment. Then the calibration and verification are carried out for each one. Finally, statistical analyses are performed to evaluate the capacity of the prototypes to discriminate among different tested concentrations. After analysing the results, we discussed the two

major findings of the presented results. First, the effects of changing the configuration on the WF, on Vout, and on its capability to serve as a sensor are discussed. Then, the observed different tendency between Vout and concentration before and after the PF was analysed and compared with the results of other papers. As a final point, we compared the results of the three prototypes, according to the requirements set at the beginning of the paper, to determine which was the best prototype and configuration. The third prototype with the first configuration was the selected one.

In future work, we intend to make an in-depth analytical study of the influence of electrics parameters, such as permeability and permittivity, in electromagnetic fields, by applying the green function in quasi-static conditions [42]. Moreover, we are going to study the effect of water temperature. Although in other papers, authors do not find any effect from 1 to 20 °C in soil measures, we have a different medium and higher temperatures. If an effect of temperate is detected, we will develop calibration curves for different temperatures. Moreover, the use of secondary sensors, such as optical sensor will be proposed, and other types of fertilisers will be tested. Finally, theoretical and electrical models will be made to describe the inductance and an internal resistance, in series with an induced resistance due to the conduction losses in the medium, and an additional inductance due to the permittivity and permeability of the medium.

Author Contributions: Conceptualisation, J.L.; methodology, L.P. and M.B.-C.; field measures and sampling, D.A.B.; data curation, L.P. and D.A.B.; writing—original draft preparation, D.A.B.; writing—review and editing, L.P., J.L. and P.V.M.; supervision, P.V.M. and J.L.; validation, P.V.M. and J.L.; project administration, J.L. All authors have read and agreed to the published version of the manuscript.

Funding: This work is partially funded by the Conselleria de Educación, Cultura y Deporte with the Subvenciones para la contratación de personal investigador en fase postdoctoral, grant number APOSTD/2019/04, by the European Union, through the ERANETMED (Euromediterranean Cooperation through ERANET joint activities and beyond) project ERANETMED3-227 SMARTWATIR, and by the European Union with the "Fondo Europeo Agrícola de Desarrollo Rural (FEADER) – Europa invierte en zonas rurales", the MAPAMA, and Comunidad de Madrid with the IMIDRA, under the mark of the PDR-CM 2014-2020" project number PDR18-XEROCESPED.

Conflicts of Interest: The authors declare no conflict of interest.

References

1. Food and Agriculture Organization. World agriculture 2030: Main Findings. Available online: http://www.fao.org/english/newsroom/news/2002/7833-en.html (accessed on 18 January 2020).
2. Bardgett, R.D.; De Vries, F.T.; Van Der Putten, W.H. Soil Biodiversity and ecosystem functioning. In *Microbial Biomass: A Paradigm Shift in Terrestrial Biogeochemistry*; World Scientific Publishing Co.: Singapore, 2017; pp. 119–140.
3. Department of Primary Industries. Plant Nutrients in the Soil. Available online: https://www.dpi.nsw.gov.au/agriculture/soils/impro vement/plant-nutrients (accessed on 18 January 2020).
4. Gamarra Lezcano, C.C.; Diaz Ortíz, M.I.; Galeano, M.P.; Cabrera Cardús, A.J. Relación carbon-nitrógeno en suelos de Sistemas silvopastoriles del Chaco paraguayo. *Rev. Mex. De Cienc. For.* **2018**, *9*, 46, doi:10.29298/rmcf.v9i46.134.
5. Gellings, C.W.; Parmenter, K.E. Energy efficiency in fertiliser production and use. Efficient Use and Conservation of Energy. In *Encyclopedia of Life Support Sytems*; Gellings, C.W., Ed.; IFA: Rome, Italy, 2016; pp. 123–136.
6. Eric Sideman. Too Much Organic Matter. Available online: https://www.mofga.org/Publications/The-Maine-Organic-Farmer-Gardener/Fall-2009/Organic-Matter (accessed on 18 January 2020).
7. Khan, M.N.; Mobin, M.; Abbas, Z.K.; Alamri, S.A. Fertilizers and their contaminants in soils, surface, and groundwater. *Encycl. Anthr.* **2018**, *5*, 225–240, doi:10.1016/B978-0-12-409548-9.09888-2.
8. Omer, N.H. Water Quality Parameters. In *Water Quality-Science, Assessments, and Policy*; IntechOpen: London, UK, 2019.

9. Kassim, M.R.M.; Mat, I.; Harun, A.N. Wireless Sensor Network in precision agriculture application. In Proceedings of the 2014 International Conference on Computer, Information and Telecommunication Systems (CITS), Jeju, South Korea, 7–9 July 2014; IEEE: New York, NY, USA, 2014; pp. 1–5.
10. Gebbers, R.; Adamchuk, V.I. Precision agriculture, and food security. *Science* **2010**, *327*, 828–883.
11. Rao, V.K.P. Fertilizer monitoring using micromachined cantilever. *Agric. Sci. Technol.* **2019**, *11*, 217–220.
12. Hirono, Y.; Nakamura, S.; Sano, T.; Nonaka, K. Monitoring and Modeling of Nitrogen Leaching Caused by Nitrogen Fertiliser Application to Green Tea Fields in Japan. In Proceedings of the 7th International Nitrogen Initiative Conference, Melbourne, Australia, 4–8 December 2016.
13. Feng, C.; Lü, S.; Gao, C.; Wang, X.; Xu, X.; Bai, X.; Wu, L. Smart fertiliser with temperature- and-pH – responsive behavior via surface-initiated polymerisation for controlled release of nutrients. *ACS Sustain. Chem. Eng.* **2015**, *3*, 3157–3166.
14. Ni, B.; Liu, M.; Lu, S.; Xie, L.; Wang, Y. Environmentally friendly slow-release nitrogen fertilisers. *J. Agric. Food Chem.* **2011**, *59*, 10169–10175.
15. Souza, C.F.; Faez, R.; Bacalhau, F.B.; Bacarín, M.F.; Pereira, T.S. In situ monitoring of controlled reléase of fertilizers in lettuce crop. *Eng. Agrícola* **2017**, *37*, 656–664.
16. Sharma, M.O.; Sonwane, P.M. Remote monitoring, and control for liquid fertiliser and wáter irrigation. In Proceedings of the 2017 International Conference on Computation of Power, Energy Information and Communication (ICCPEIC), Hong Kong, China, 22–23 March 2017; IEEE: New York, NY, USA, 2017; pp. 516–521.
17. Zhang, P.; Zhang, Q.; Liu, F.; Li, J.; Cao, N.; Song, C. The Construction of the Integration of Water and Fertilizer Smart Water Saving Irrigation System Based on Big Data. In Proceedings of the 2017 IEEE International Conference on Computational Science and Engineering (CSE) and IEEE International Conference on Embedded and Ubiquitous Computing (EUC), Guangzhou, China, 21–24 July 2017.
18. Merten, G.H.; Capel, P.D.; Minella, J.P. Effects of suspended sediment concentration and grain size on three optical turbidity sensors. *J. Soils Sediments* **2014**, *14*, 1235–1241.
19. Sänket, R.J.; Baviskar, A.; Ahire, S.S.; Mapare, S.V. Development of a low-cost nitrate detection soil sensor. In Proceedings of the 2017 International Conference on Wireless Communications, Signal Processing and Networking (WiSPNET), Chennai, India, 22–24 March 2017; pp. 1272–1275.
20. Rocher, J.; Basterrechea, D.A.; Parra, L.; Lloret, J. A New Conductivity Sensor for Monitoring the Fertigation in Smart Irrigation Systems. In *International Symposium on Ambient Intelligence*; Springer: Cham, Switzerland, 2019; pp. 136–144.
21. Nor, A.S.M.; Yunus, M.A.M.; Nawawi, S.W.; Ibrahim, S. Low-cost sensor array design optimisation based on planar electromagnetic sensor design for detecting nitrate and sulfate. In Proceedings of the 2013 Seventh International Conference on Sensing Technology (ICST), Wellington, New Zealand, 3–5 December 2013; IEEE: New York, NY, USA, 2013; pp. 693–698.
22. Comsol Multiphysics. Available online: https://www.comsol.com/ (accessed on 10 September 2020).
23. Griffin, D.D.; Chew, W.C.; Clark, B.; Kleinberg, R.L. Apparatus for microinductive investigation of earth formations with improved electroquasistatic shielding. U.S. Patent 4,739,272, 19 April, 1988.
24. Kleinberg, R.L.; Chew, W.C.; Griffin, D.D. Noncontacting electrical conductivity sensor for remote hostile environments. *IEEE Trans. Instrum. Meas.* **1989**, *38*, 22–26.
25. Parra-Boronat, L.; Marín, J.; Ablanque, M.; Mauri, P.V.; Lloret, J.; Torices, V.; Massager, A. Scatternet Formation Protocol for Environmental Monitoring in a Smart Garden. *Netw. Protoc. Algorithms* **2018**, *10*, 63–84.
26. Poljak, D.; Cvetković, M. *Human Interaction with Electromagnetic Fields: Computational Models in Dosimetry*; Academic Press: Cambridge, MA, USA, 8 June 2019; pp. 53–89.
27. Wood, L.T.; Rottmann, R.M.; Barrera, R. Faraday's law, Lenz's law, and conservation of energy. *Am. J. Phys.* **2004**, *72*, 376, doi:10.1119/1.1646131.
28. Wood, R.T.; Bannazadeh, A.; Nguyen, Q.; Bushnell, L.G. A salinity sensor for long-term data collection in estuary studies. In Proceedings of the OCEANS 2010 MTS/IEEE SEATTLE, Seatle, WA, USA, 20–23 September, 2010.
29. Parra, L.; Sendra, S.; Lloret, J.; Bosch, I. Development of a Conductivity Sensor for Monitoring Groundwater Resources to Optimise Water Management in Smart City Environments. *Sensors* **2015**, *15*, 20990–21015.

30. Pham, T.T.; Green, T.; Chen, J.; Truong, P.; Vaidya, A.; Bushnell, L. A salinity sensor system for estuary studies. In Proceedings of the IEEE OCEANS 2008, Quebec City, QC, Canada, 15–18 September 2008.
31. Parra, M.; Parra, L.; Rocher, J.; Lloret, J.; Mauri, P.V.; Linares, J.V. A Novel Low-Cost Conductivity Based Soil Moisture Sensor. In *International Conference on Advanced Intelligent Systems for Sustainable Development*, Springer: Cham, Switzerland, 2019; pp. 27–35.
32. García-Navas, J.L.; Parra, M.; Parra, L.; Rocher, J.; Sendra, S.; Lloret, J. Practical Study of the Temperature Effect in Soil Moisture Measurements, 2019. In Proceedings of the Eighth International Conference on Communications, Computation, Networks and Technologies (IARIA), Valencia, Spain, 24–28 November 2019; pp. 7–13.
33. Rocher, J.; Basterrechea, D.A.; Taha, M.; Parra, M.; Lloret, J. Water Conductivity Sensor based on Coils to Detect Illegal Dumpings in Smart Cities, 2019. In Proceedings of the Fourth International Conference on Fog and Mobile Edge Computing (FMEC), Rome, Italy, 10–13 June 2019; IEEE: New York, NY, USA, 2019; pp. 324–329.
34. Karagianni, E.A. Electromagnetic Waves under Sea: Bow-Tie Antenna Design for Wi-Fi Underwater Communications. *Prog. Electromagn. Res. M* **2015**, *41*, 189–198.
35. Tektronix. Available online: https://www.tek.com/signal-generator/afg1022 (accessed on 5 December 2019).
36. Tektronix. Available online: https://www.tek.com/oscilloscope/tbs1104 (accessed on 5 December 2019).
37. Crison. Available online: http://www.crisoninstruments.com/es/laboratorio/conductimetro/desobremesa/ec-metro-basic-30 (accessed on 6 December 2019).
38. Leroy Merlin. Available online: https://www.leroymerlin.es/fp/19468554/fertilizante-para-citricos-geolia-uso-ecologico-1l (accessed on 12 July 2020).
39. Statgraphics. Available online: https://statgraphics.net/descargas-centurion-xvii/ (accessed on 16 January 2020).
40. Matsoukis, A.; Kamoutsis, A.; Chronopoulou Sereli, A. A note on the flowering of Ajuga orientalis L. in relation to air temperature in Mount Aenos (Cephalonia, Greece). *Curr. Agric. Res. J.* **2018**, *6*, 261–267.
41. Sokal, R.R. The principles and practice of statistics in biological research. *Biometry* **1995**, *56*, 451–554.
42. Calle, H.B. Green Function Theory of Ferromagnetism. *Phys. Rev.* **1963**, *130*, 3.